

Spin-dependent heat and thermoelectric currents in a Rashba ring coupled to a photon cavity

Nzar Rauf Abdullah¹, Chi-Shung Tang², Andrei Manolescu³
and Vidar Gudmundsson⁴

¹Physics Department, College of Science, University of Sulaimani, Kurdistan Region, Iraq

² Department of Mechanical Engineering, National United University, 1, Lienda, Miaoli 36003, Taiwan

³ Reykjavik University, School of Science and Engineering, Menntavegur 1, IS-101 Reykjavik, Iceland

⁴ Science Institute, University of Iceland, Dunhaga 3, IS-107 Reykjavik, Iceland

E-mail: nzar.r.abdullah@gmail.com, vidar@hi.is

Abstract. Spin-dependent heat and thermoelectric currents in a quantum ring with Rashba spin-orbit interaction placed in a photon cavity are theoretically calculated. The quantum ring is coupled to two external leads with different temperatures. In a resonant regime, with the ring structure in resonance with the photon field, the heat and the thermoelectric currents can be controlled by the Rashba spin-orbit interaction. The heat current is suppressed in the presence of the photon field due to contribution of the two-electron and photon replica states to the transport while the thermoelectric current is not sensitive to changes in parameters of the photon field. Our study opens a possibility to use the proposed interferometric device as a tunable heat current generator in the cavity photon field.

PACS numbers: 78.20.N-, 73.23.-b, 42.50.Pq, 78.20.Jq

1. Introduction

Thermal properties of nanoscale systems have attracted much interest due to their high efficiency of converting heat into electricity [1] which has been studied by both experimental [2] and theoretical [3] groups. This growing interest in thermal properties on the nanoscale is mainly caused by the peculiar thermal transport behaviors of the systems, which follow from their very special electronic structure. Traditionally, thermal transport can be obtained by a temperature gradient across a system that contains mobile charge, which in turn create a thermoelectric current (TEC) [4]. Detailed experimental and theoretical tests have provided new insight into the thermoelectrics of low dimensional structures such as quantum dots [5, 6, 7], double quantum dots [8], quantum point contacts [9, 10], quantum wires [11], and quantum rings [12, 13]. These nano-structures show that high thermoelectric efficiency may be achieved by using the quantum properties of the systems [1], such as quantized energy [14], and interference effects [15].

On the other hand, it has been shown that the spin polarization induced by an electric field in a two-dimensional electron gas with a Rashba spin-orbit interaction influences the thermal transport [16]. This phenomenon has been investigated in various systems exhibiting Rashba spin-orbit interaction [17, 18]. In this system, the temperature gradient is utilized as a possibility to generate spin-dependent thermoelectric and heat currents, in an analogy to the generation of a charge current in conventional thermoelectrics.

Until now, earlier work focused mostly on thermal transport without the influences of a cavity photon field on the electronic structure. In a previous paper, we studied the influences of a quantized photon field on TEC [19]. We assumed a quantum wire coupled to a photon cavity and found that the TEC strongly depends on the photon energy and the number of photons initially in the cavity. In addition, the current is inverted for the off-resonant regime and a reduction in the current is found for a photon field in resonance to electronic systems, a direct consequence of the Rabi-splitting. In the present work, we study the thermoelectric effect in a quantum ring taking into account the electron-electron and electron-photon interactions in the presence of a Rashba spin-orbit coupling. The spin-dependent heat and thermoelectric currents are calculated using the generalized non-Markovian master equation when the bias voltage difference between the two leads tends to zero. Moreover, the influences of the photon field on thermal transport of the system is presented. We investigate these effects in the late transient time regime before the photon leak of the cavity influences the results.

2. Theory

We model the thermal properties of the quantum device based on a quantum ring coupled to a cavity photon field. The quantum ring is assumed to be realized in a two dimensional electron gas of an GaAs/AlGaAs hetero-structure in the xy -plane and the

photon field is confined to a three-dimensional cavity. The quantum ring is embedded in a cavity that is much larger than the ring. In addition, the quantum ring is diametrically coupled to two semi-infinite leads.

2.1. Quantum ring coupled to a cavity photon field

The quantum ring embedded in the central system with length $L_x = 300$ nm is schematically shown in Fig. 1. The ring is parabolically confined with characteristic

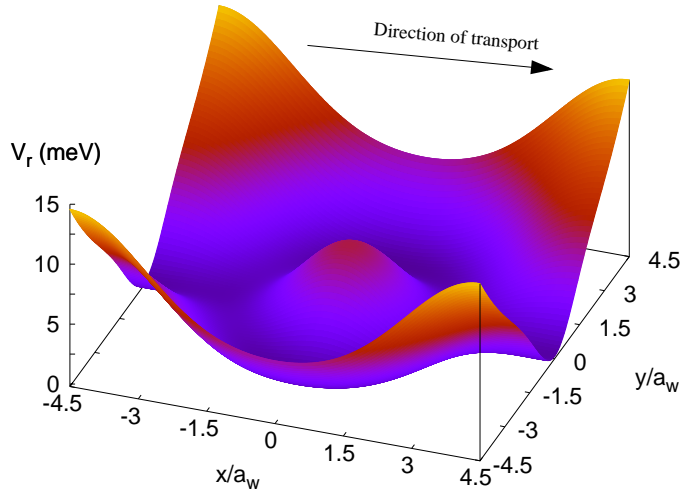


Figure 1. (Color online) The potential $V_r(\mathbf{r})$ defining the central ring system that will be coupled diametrically to the semi-infinite left and right leads in the x -direction.

energy $\hbar\Omega_0 = 1.0$ meV along the y -direction and hard-wall confined in the transport direction (x -direction). The potential of the ring is expressed as

$$V_r(\mathbf{r}) = \sum_{i=1}^6 V_i \exp [- (\gamma_{xi}(x - x_{0i}))^2 - (\gamma_{yi}y)^2] + \frac{1}{2}m^*\Omega_0^2y^2, \quad (1)$$

where V_i , γ_{xi} , and γ_{yi} are constants presented in Table 1. $x_{03} = \epsilon$ is a small numerical symmetry breaking parameter with $|\epsilon| = 10^{-5}$ nm to guarantee a numerical stability. The second term of Eq. (1) indicates the characteristic energy of the electron confinement of the short quantum wire the quantum ring is embedded in.

The central system is coupled to a photon cavity much larger than the central system. The total momentum operator of the quantum ring coupled to the photon field is defined as

$$\hat{\mathbf{p}}(\mathbf{r}) = \frac{\hbar}{i}\nabla + \frac{e}{c} \left[\hat{\mathbf{A}}(\mathbf{r}) + \hat{\mathbf{A}}_\gamma(\mathbf{r}) \right], \quad (2)$$

where $\hat{\mathbf{A}}(\mathbf{r}) = -By\hat{x}$ is the vector potential of the static classical external magnetic field with $\mathbf{B} = B\hat{z}$, and $\hat{\mathbf{A}}_\gamma(\mathbf{r})$ is the vector potential of the quantized photon field in

Table 1. Constants of the ring potential.

| i | V_i (meV) | γ_{xi} (nm ⁻¹) | x_{0i} (nm) | γ_{yi} (nm ⁻¹) |
|-----|-------------|-----------------------------------|---------------|-----------------------------------|
| 1 | 10 | 0.013 | 150 | 0 |
| 2 | 10 | 0.013 | -150 | 0 |
| 3 | 11.1 | 0.0165 | ϵ | 0.0165 |
| 4 | -4.7 | 0.02 | 149 | 0.02 |
| 5 | -4.7 | 0.02 | -149 | 0.02 |
| 6 | -5.33 | 0 | 0 | 0 |

the cavity that is introduced in terms of the photon creation (\hat{a}^\dagger) and annihilation (\hat{a}) operators

$$\hat{\mathbf{A}}_\gamma = A(\mathbf{e}\hat{a} + \mathbf{e}^*\hat{a}^\dagger) \quad (3)$$

with $\mathbf{e} = \mathbf{e}_x$ for the longitudinal photon polarization (x -polarization) and $\mathbf{e} = \mathbf{e}_y$ for the transverse photon polarization (y -polarization) [20].

The Hamiltonian for two-dimensional electrons in the quantum ring coupled to a photon cavity is

$$\begin{aligned} \hat{H}_S = \int d^2r \hat{\Psi}^\dagger(\mathbf{r}) \left[\left(\frac{\hat{\mathbf{p}}^2}{2m^*} + V_r(\mathbf{r}) \right) + H_Z + \hat{H}_R(\mathbf{r}) \right] \hat{\Psi}(\mathbf{r}) \\ + \hat{H}_{ee} + \hbar\omega\hat{a}^\dagger\hat{a}, \end{aligned} \quad (4)$$

with the electron spinor field operators

$$\hat{\Psi}(\mathbf{r}) = \begin{pmatrix} \hat{\Psi}(\uparrow, \mathbf{r}) \\ \hat{\Psi}(\downarrow, \mathbf{r}) \end{pmatrix}, \quad \hat{\Psi}^\dagger(\mathbf{r}) = \left(\hat{\Psi}^\dagger(\uparrow, \mathbf{r}), \hat{\Psi}^\dagger(\downarrow, \mathbf{r}) \right), \quad (5)$$

where $\hat{\Psi}(x) = \sum_a \psi_a^S(x) \hat{C}_a$ is the field operator with $x \equiv (\mathbf{r}, \sigma)$, $\sigma \in \{\uparrow, \downarrow\}$ and the annihilation operator, \hat{C}_a , for the single-electron state (SES) $\psi_a^S(x)$ in the central system. The second term of Eq. (4) is the Hamiltonian that gives the Zeeman interaction of the static magnetic field with spin of the electron. It can be described by $H_Z = \frac{1}{2}(\mu_B g_S B \sigma_z)$, where μ_B is the Bohr magnetron and g_S refers to the electron spin g-factor. The third terms of Eq. (4) is the Rashba-spin orbit coupling that describes the interaction between the orbital motion and the spin of an electron

$$\hat{H}_R(\mathbf{r}) = \frac{\alpha}{\hbar} (\sigma_x \hat{p}_y(\mathbf{r}) - \sigma_y \hat{p}_x(\mathbf{r})), \quad (6)$$

where α is a coupling constant that can be tuned by an external electric field, and σ_x and σ_y are the Pauli matrices. In addition, \hat{H}_{ee} stands for the electron-electron interaction [21, 22, 23], and $\hbar\omega_\gamma\hat{a}^\dagger\hat{a}$ is the free photon Hamiltonian in the cavity with $\hbar\omega_\gamma$ as the photon energy.

A time-convolutionless generalized master equation (TCL-GME) is utilized to investigate the transport properties of the system [24, 25, 26]. The TCL-GME is local in time and satisfies the positivity for the many-body state occupation described the

reduced density operator (RDO). Before the central system is coupled to the leads, the total density matrix is the product of the density matrices of the system and the leads $\hat{\rho}_T$. The RDO of the system after the coupling is defined as The reduced density operator is calculated using a TCL non-Markovian generalized master equation (GME) valid for a weak coupling of the leads and system. The GME is derived according to a Nakajima-Zwanzig projection approach with the coupling Hamiltonian entering the dissipation kernel of the integro-differential equation up to second order. The coupling of the central system and the leads is expressed by a many-body coupling tensor derived from the geometry of the single-electrons states in the contact area of the leads and system [27, 28].

$$\hat{\rho}_S(t) = \text{Tr}_l(\hat{\rho}_T) \quad (7)$$

where $l \in \{L, R\}$ refers to the two electron reservoirs, the left (L) and the right (R) leads, respectively. The time needed to reach the steady state depends on the chemical potentials in each lead, the bias window, and their relation to the energy spectrum of the system. In our calculations we integrate the GME to $t = 220$ ps, a point in time late in the transient regime when the system is approaching the steady state.

The heat current (I^H) can be calculated from the reduced density operator. It is the rate at which heat is transferred through the system over time. Therefore, the heat current in our system can be introduced as

$$\begin{aligned} I_t^H &= c_l \frac{d}{dt} \left[\hat{\rho}_{S,l}(t) (\hat{H}_S - \mu \hat{N}_e) \right] \\ &= c_l \sum_{\alpha\beta} (\hat{\alpha} | \dot{\hat{\rho}}_{S,l} | \hat{\beta}) (E_\alpha - \mu \hat{N}_e) \delta_{\alpha\beta}, \end{aligned} \quad (8)$$

where $\hat{\rho}_{S,l}$ is the reduced density operator in terms of the l lead, $c_L = +1$, but $c_R = -1$, and \hat{H}_S is the Hamiltonian of the central system coupled to a cavity, $\mu = \mu_L = \mu_R$, and \hat{N}_e is the number operator of the electrons in the ring system. The thermoelectric current (I^{TH}) in terms of the reduced density operator can be defined as

$$I_t^{\text{TH}} = c_l \text{Tr}[\dot{\hat{\rho}}_{S,l} \hat{Q}], \quad (9)$$

where the charge operator is $\hat{Q} = e \int d^2r \hat{\Psi}^\dagger(\mathbf{r}) \hat{\Psi}(\mathbf{r})$ [27, 28].

In the next section, we present our main results of the thermal transport of a quantum ring coupled to a photon field.

3. Results

We assume a single cavity mode with photon energy $\hbar\omega_\gamma = 0.55$ meV. The applied perpendicular magnetic field is $B = 10^{-5}$ T to lift the spin degeneracy. The value of the magnetic field is out of the Aharonov-Bohm (AB) regime because the area of the ring structure is $A = \pi a^2 \approx 2 \times 10^4$ nm² leading to a magnetic field $B_0 = \phi_0/A \approx 0.2$ T corresponding to one flux quantum $\phi_0 = hc/e$ [25]. The applied magnetic field is $B = 10^{-5}$ T is much smaller than B_0 , orders of magnitudes outside the AB regime.

A temperature difference is applied between the left and the right leads, which induces a current to flow in the central system. A temperature gradient emerges as the leads are coupled with different thermal baths. Therefore, a thermal current is driven to flow through the ring due to the Seebeck effect.

We begin our description by showing the energy spectrum of the ring versus the Rashba coupling constant in Fig. 2, where the states 0ES (green rectangles) are zero-electron states, 1ES (red circles) are one-electron states, and 2ES (blue circles) are two-electron states. Figure 2(a) displays the many-electron energy of the quantum ring

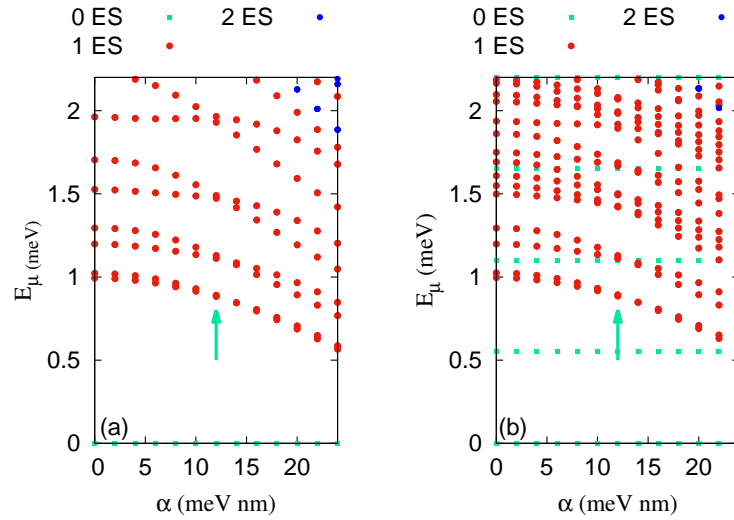


Figure 2. (Color online) Energy spectra (E_μ) of the ring system as a function of the Rashba coupling constant α without (a), and with (b) a photon cavity. The states 0ES (green rectangles) are zero-electron states, 1ES (red circles) are one-electron states, and 2ES (blue circles) are two-electron states. The photon energy is $\hbar\omega_\gamma = 0.55$ meV, the electron-photon coupling strength is $g_\gamma = 0.05$ meV, and the photons are linearly polarized in the x -direction. The magnetic field is $B = 10^{-5}$ T, and $\hbar\Omega_0 = 2.0$ meV.

without a cavity photon field. The energy of the states decreases with increasing Rashba coupling constant. As a result, crossing of the one-electron states at $\alpha \approx 12$ meV (green arrow) are formed corresponding to the AC destructive phase interference [25].

Figure 2(b) displays an energy spectrum of photon-dressed many-body states of the quantum ring in the presence of the photon field with energy $\hbar\omega_\gamma = 0.55$ meV and coupling $g_\gamma = 0.05$ meV. Comparing to the energy spectrum in Fig. 2(a), where the photon field is neglected, photon replica states are formed. The energy spacing between the photon replicas is approximately equal to the photon energy at low electron-photon coupling strength. Generally, the perturbational idea of a simple replica with an integer photon number only applies for a weakly coupled electrons and photons out of resonance, but we use here the terminology to indicate the more general concept of cavity-photon dressed electron states. For instance at the Rashba coupling constant $\alpha = 0.0$ meV nm, the state at $E_\mu \simeq 1.5$ meV, the first replica of the ground state, is formed near the second-excited state that can not be seen in the absence of the photon field (Fig.

2(a)). The ring system here under this condition is in a resonance with the photon field. These photon replicas have an important role in the electron transport through the system that will be shown later. In addition, the energy spectrum of the leads has a subband structure (not shown) since the leads contain semi-infinite quasi-one-dimensional non-interacting electron systems [23].

3.1. Heat current

Heat current is the rate of change in the thermal energy as it is presented in Eq. (8). In nanoscale systems coupled to electron reservoirs with zero bias window, the heat current takes on zero or positive values depending on the location of the chemical potential of the leads with respect to the energy states of the system. If the chemical potential is equal to the value of the energy of an *isolated* state of the system, the quantum system is resonant with the leads, and the heat current is close to zero as is seen in quantum dots [6]. Otherwise, the heat current has a positive value. We observe that for our rather large ring structure the heat current has always a nonvanishing positive value. This has to do with the high density of states or the near degeneracy of the states of the system, that the tiny Zeeman spin term or the Rashba spin-orbit coupling in the ring does not drastically change. Important here is the thermal energy due to the higher temperature in the left lead and the photon energy with respect to the energy scale of the rings. They are all of a similar order.

Figure 3 indicates the heat current versus the chemical potential of the leads for three different values of the Rashba coupling constant: $\alpha = 0.0$ (blue squares), $\alpha = 6.0$ (red circles), and $\alpha = 12.0$ meV nm (green diamonds). As we see, the heat current is zero below $\mu = 1.0$ meV because this region is below the lowest subband energy of the leads.

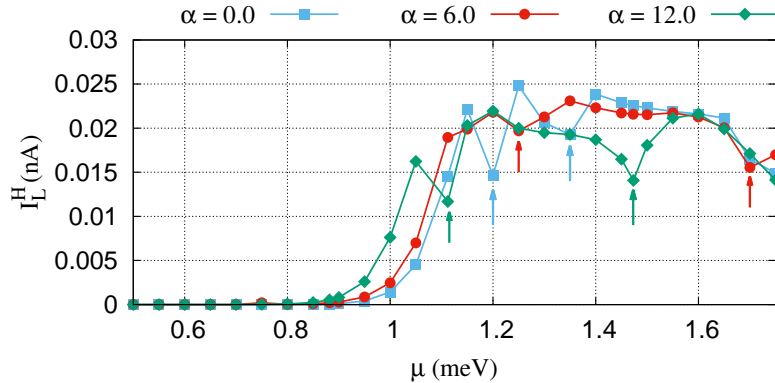


Figure 3. (Color online) The heat current versus the chemical potential of the leads for three different values of the Rashba coefficient: $\alpha = 0.0$ (blue squares), $\alpha = 6.0$ (red circles), and $\alpha = 12.0$ meV nm (green diamonds). The temperature of the left (right) lead is fixed at $T_L = 0.41$ K ($T_R = 0.01$ K) implying thermal energy $k_B T_L = 0.35$ meV ($k_B T_R = 0.00086$ meV), respectively. The magnetic field is $B = 10^{-5}$ T and $\hbar\Omega_0 = 1.0$ meV.

In the absence of the Rashba spin-orbit interaction ($\alpha = 0.0$ meV nm), for the selected range of the chemical potentials from $\mu = 1.0$ to 1.75 meV, we observe 6 photon dressed electron states, the lowest of which is the ground state as is shown in Fig. 2(a). Therefore, a change of the chemical potential μ brings these ring states into resonance with the leads. For the low magnetic field the two spin components of these states are almost degenerate and the ring structure supplies a further near orbital degeneracy giving the heat current a nonzero value at the above mentioned resonant states. Two current dips (blue arrows) are formed at $\mu = 1.2$ and 1.35 meV corresponding to the second- and third-excited states, respectively.

In the presence of the Rashba spin-orbit interaction when $\alpha = 6.0$ meV nm (red circles) two current dips are observed at $\mu = 1.25$ and 1.70 meV corresponding to the third- and fifth-excited states, respectively. Tuning the Rashba coupling constant to $\alpha = 12.0$ meV nm (green diamonds) the two dips are formed at $\mu = 1.112$ and 1.473 meV corresponding to an additional degeneration of the second- and third-excited states on one hand, and the fourth- and fifth-excited states on the other hand. In this case, the strong degeneration caused by the Rashba spin-orbit interaction induces a smaller heat current in the dips compared to the current dip at $\alpha = 6.0$ meV nm.

The results here are very interesting because the nonzero heat current at the resonant energy levels can only be obtained in systems with high density of states (or near degeneracy) offered by the ring structure, the smaller the Zeeman spin-splitting, or the Rashba spin-orbit interaction. We also notice that in the all aforementioned cases the two-electron states are active in the transport in such a way, that one fourth of the heat current is carried by the two-electron states. It should be mentioned that the mechanism of transferred heat current through the one- and two-electron states is different here. The heat current flows from the left lead to the ring system through the one-electron states, but the opposite mechanism happens in the case of the two-electron states, where the heat current is transferred from the ring to the left lead. Therefore, the contribution of the two electron-states reduces the “total” heat current in the system for the range of the chemical potential used here.

Now, we consider the ring to be coupled to a cavity with x -polarized photon field, and initially no photon in the cavity. To see the influences of the photon field on the heat current, we tune the electron-photon coupling strength g_γ and fix the Rashba coupling constant at $\alpha = 12.0$ meV nm (degenerate states). Figure 4(a) displays the heat current as a function of the chemical potential for different values of the electron-photon coupling strength g_γ . It is clearly seen that in the presence of the photon field the heat current is almost unchanged around $\mu = 1.112$ meV (left green arrow) corresponding to the degeneracy point of the second- and third-excited states at $E_\mu = 1.112$ meV since they are off-resonance states with respect to the photon field. But, the heat current is suppressed at the degenerate energy of the fourth- and fifth-excited states $E_\mu = 1.473$ meV due to the activated photon replica states in the transport. The photon energy is $\hbar\omega_\gamma = 0.55$ meV which is approximately equal to the energy spacing between the ground state/first-excited state and the fourth-/fifth-excited states, respectively.

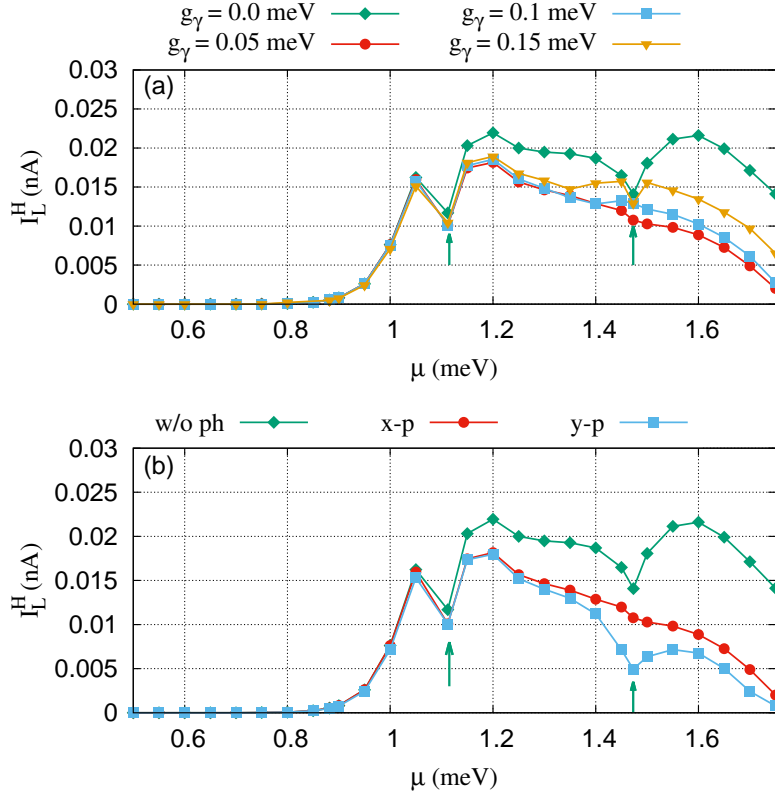


Figure 4. (Color online) Shows the heat current versus the chemical potential with $\alpha = 12$ meV, and $\hbar\omega_\gamma = 0.55$ meV. The green arrows indicate the current dip at the resonant energy levels. (a) The heat current is plotted for $g_\gamma = 0.0$ meV without the photon field (green diamonds) and $g_\gamma = 0.05$ meV (red circles), $g_\gamma = 0.1$ meV (blue rectangles), and $g_\gamma = 0.15$ meV (golden triangles) with the photon field. (b) The heat current for the system without the photon field w/o ph (green diamonds) and with the photon field for x- (red circles) and y-polarization (blue rectangles) is shown when $g_\gamma = 0.05$ meV. The temperature of the left (right) lead is fixed at $T_L = 0.41$ K ($T_R = 0.01$ K) implying thermal energy $k_B T_L = 0.35$ meV ($k_B T_R = 0.00086$ meV), respectively. The magnetic field is $B = 10^{-5}$ T and $\hbar\Omega_0 = 1.0$ meV.

However the contribution of the photon replica states is weak here because the cavity contains no photon initially, but it influences the heat current in the system. In addition, the contribution of the one-electron (two-electron) states to the transport in the presence of the photon field is decreased (increased), respectively. As a result, the heat current is suppressed in the system.

We tune the photon polarization to the y -direction and see the contribution of the two-electron states to the transport is further enhanced. Thus, the heat current is again suppressed as is shown in Fig. 4(b) (blue rectangles).

The temperature dependence of the heat current for all three considered electron-photon coupling strengths is shown in Fig. 5 when the Rashba coupling constant is $\alpha = 12.0$ meV nm and $\mu = 1.112$ meV (at the degenerate energy level of the second- and the third-excited states). We fix the temperature of the right lead at $T_R = 0.01$ K

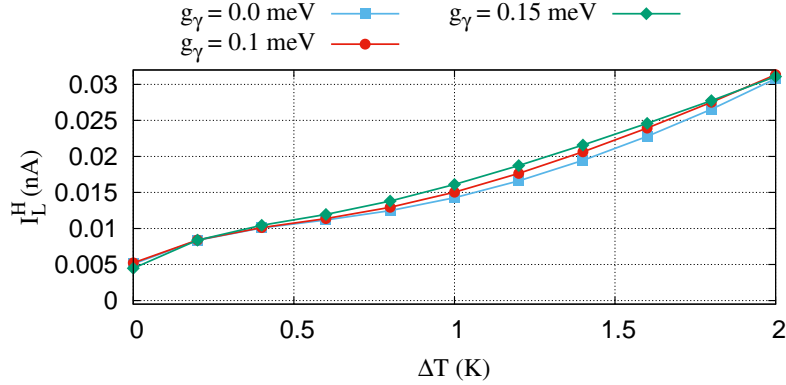


Figure 5. (Color online) Heat current versus the temperature gradient of the leads is shown for three different values of the electron-photon coupling: $g_\gamma = 0.0$ meV (blue rectangles) $g_\gamma = 0.1$ meV (red circles), $g_\gamma = 0.15$ meV (green diamonds). The temperature of the right lead is fixed at $T_R = 0.01$ K and tune the temperature of the left lead. The Rashba coupling constant is $\alpha = 12.0$ meV nm (degeneracy energy point), the chemical potential of the leads are $\mu_L = \mu_R = 1.112$ meV, the magnetic field is $B = 10^{-5}$ T and $\hbar\Omega_0 = 1.0$ meV.

and tune the temperature of the left lead. The heat current increases by enhancement of the temperature because the electrons carry more thermal energy. As is expected the heat current is not significantly changed by tuning the strength of the electron-photon coupling because the energy states at $E_\mu = 1.112$ meV are out of resonance with respect to the photon field as we mentioned above.

3.2. Thermoelectric current

A temperature gradient causes a current to flow along a quantum ring. The electrons move from the hot lead to the cold lead, but also from the cold to the hot one, depending on the position of the chemical potential relatively to the energy spectrum of the central system. Both electron and energy are transported in this case [6]. The movement of electrons under the temperature gradient induces the TEC. We show how the TEC defined in Eq. (9) is influenced by the Rashba spin-orbit interaction and the photon field. Figure 6(a) indicates the TEC versus the chemical potential of the leads for three different values of the Rashba coupling constant: $\alpha = 0.0$ (blue squares), $\alpha = 6.0$ (red circles), and $\alpha = 12.0$ meV nm (green diamonds).

The TEC is essentially governed by the difference between the two Fermi functions of the external leads. The TEC is generated when the Fermi functions of the leads have the same chemical potential but different width. One can explain the TEC of the system when $\alpha = 0.0$ meV nm in the following way: The TEC becomes zero in two cases. First, when the two Fermi functions or the occupations are equal to 0.5 (half filling), and in the second one, both Fermi functions imply occupations of 0 or 1 (integer filling), as is shown in Fig. 6(b) [29, 14].

Consequently, the TEC is approximately zero at $\mu \approx 1.112$ meV (blue squares)

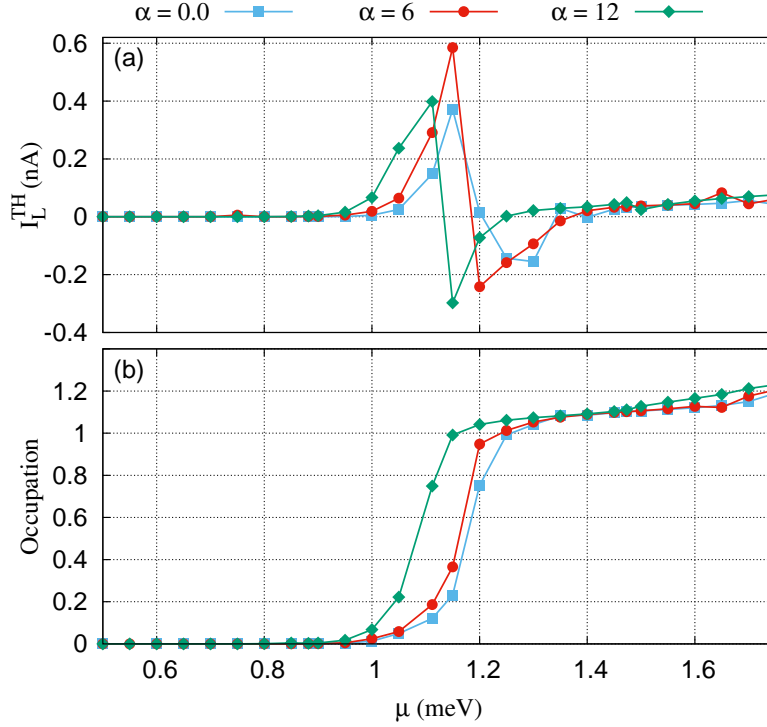


Figure 6. (Color online) TEC (I_L^{TH}) (a) and occupation (b) versus the chemical potential of the leads in the absence of the photon field for three different values of the Rashba coupling constant: $\alpha = 0.0$ (blue squares), $\alpha = 6.0$ (red circles), and $\alpha = 12.0$ meV nm (green diamonds). The temperature of the left (right) lead is fixed at $T_L = 0.41$ K ($T_R = 0.01$ K) implying thermal energy $k_B T_L = 0.35$ meV ($k_B T_R = 0.00086$ meV), respectively. The magnetic field is $B = 10^{-5}$ T and $\hbar\Omega_0 = 1.0$ meV.

corresponding to half filling of the degenerate energy levels of the second- and the third-excited state [19]. The TEC is approaching to zero at $\mu \leq 1.0$ and $\mu \geq 1.4$ meV for the integer filling of 0 and 1, respectively. The same mechanism applies to the ring system including the spin-orbit interaction when the Rashba coupling constant is $\alpha = 6.0$ (red circles) and 12.0 meV nm (green diamonds). But in the presence of the Rashba spin-orbit interaction, the TEC and the half filling is slightly shifted to the left side because the energy states are shifted down for the higher value of the Rashba coupling constant (see Fig. 2(a)). We should mention that all the states contributing to the TEC are one-electron states, while the one- and two-electron states participated in the creation the heat current.

The effects of the photon field on the TEC in the system should not be neglected. Figure 7 displays the TEC versus the chemical potential of the leads. In Fig. 7(a) the TEC is plotted for different values of the electron-photon coupling strength. Assuming the photon energy is $\hbar\omega_\gamma = 0.55$ meV, the Rashba coupling constant is fixed at $\alpha = 12$ meV nm, and the photon field is polarized in the x -direction. We can clearly see that the TEC is not efficiently influenced by tuning the electron-photon coupling

strength because the cavity is initially empty of photons. The TEC is drastically changed by tuning the number of photon initially in the cavity as shown in Ref. [19]. In addition, the TEC is not significantly affected by the direction of the photon polarization in the cavity as is shown in Fig. 7(b).

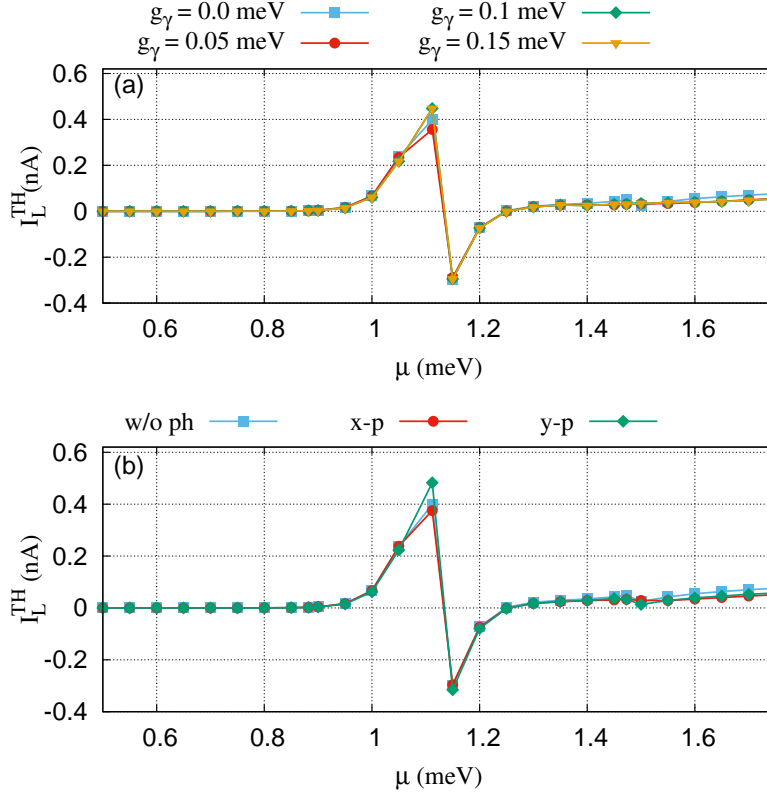


Figure 7. (Color online) Shows the TEC versus the chemical potential in the presence of the photon field with $\hbar\omega_\gamma = 0.55$ meV and the Rashba coupling constant is $\alpha = 12$ meV nm. (a) The TEC is plotted for the system without the photon field $g_\gamma = 0.0$ meV (blue rectangles) and with the photon field when $g_\gamma = 0.05$ meV (red circles), $g_\gamma = 0.1$ meV (green diamonds), and $g_\gamma = 0.15$ meV (golden triangles). The photon field is polarized in the x -direction. (b) The TEC is presented for the system without the photon field (w/o ph) (blue rectangles) and with the photon field (w ph) of x - (red circles) and y -polarization (green diamonds) when $g_\gamma = 0.05$ meV. The temperature of the left (right) lead is fixed at $T_L = 0.41$ K ($T_R = 0.01$ K) implying thermal energy $k_B T_L = 0.35$ meV ($k_B T_R = 0.00086$ meV), respectively. The magnetic field is $B = 10^{-5}$ T and $\hbar\Omega_0 = 1.0$ meV.

Variation of the TEC and the occupation with the Rashba coupling constant α are shown in Fig. 8 for the system without a photon field (w/o ph) (blue rectangles) and with the photon field (w ph) (red circles). The chemical potential is fixed at $\mu_L = \mu_R = 1.112$ meV corresponding to the degeneration point of the first- and the second-excited states at $\alpha = 12.0$ meV nm (see Fig. 2(a)). The TEC here depends on the same mechanism, whether the occupation is an integer or a half integer. Therefore, the TEC is zero at the half integer occupation around $\alpha = 12.0$ meV nm, and the TEC

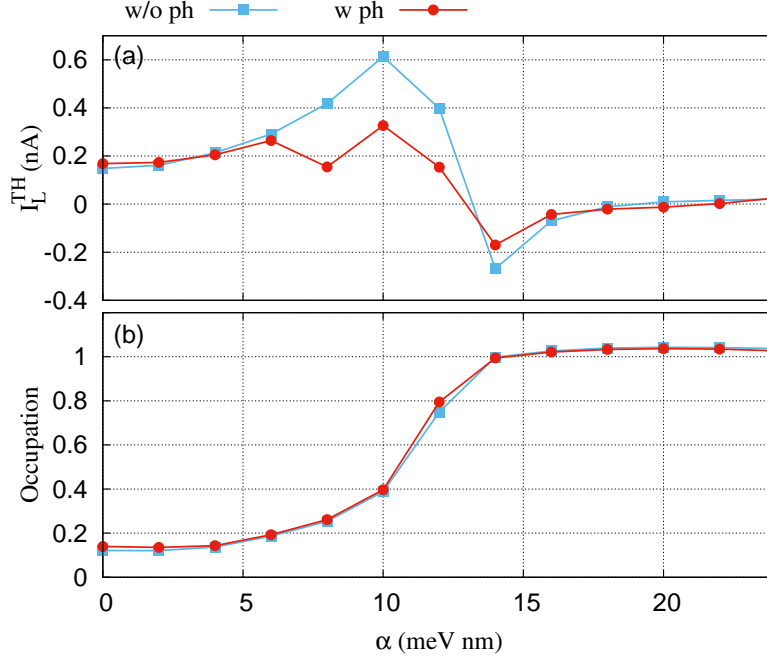


Figure 8. (Color online) TEC (a) and occupation (b) versus the chemical potential of the leads for the quantum ring without photon field (w/o ph) (blue rectangles) and with the photon field w ph (red circles). The chemical potential is fixed at $\mu_L = \mu_R = 1.112$ meV corresponding to the degenerate energy level of the first- and second-excited states at $\alpha \approx 12.0$ meV nm shown in Fig. 2. The temperature of the left (right) lead is fixed at $T_L = 0.41$ K ($T_R = 0.01$ K) implying thermal energy $k_B T_L = 0.35$ meV ($k_B T_R = 0.00086$ meV), respectively. The magnetic field is $B = 10^{-5}$ T and $\hbar\Omega_0 = 1.0$ meV.

is approximately zero at the integer occupation around $\alpha \leq 5.0$ and $\alpha \geq 15.0$ meV nm as is seen in Fig. 8(a) and (b).

Opposite to the heat current shown in Fig. 5, the TEC is slightly enhanced by a stronger electron-photon coupling strength $g_\gamma = 0.15$ meV at higher temperature gradient (see Fig. 9). It also indicates that the characteristics of the TEC are almost the same even if the temperature gradient is increased in the system up to 2.0 K.

4. Conclusions

We have investigated the thermal properties of a quantum ring coupled to a photon field, and two electron reservoirs for sequential tunneling through the system. We focused on the quantum limit where the energy spacing between successive electronic levels is larger than the thermal energy $\Delta E_\mu > k_B \Delta T$. A general master equation is used to study the time-evolution of electrons in the system. Although, one expects the heat current to be nearly zero at resonant energy levels with respect to the leads [30], our study shows that the heat current has nonzero values in the presence of the high density of states or near degeneracies caused by the ring structure and a tiny Zeeman spin splitting. A

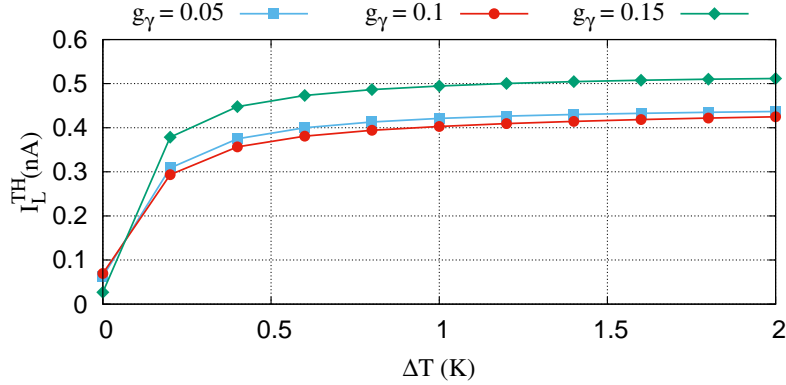


Figure 9. (Color online) TEC versus the temperature gradient of the leads is shown for three different values of the electron-photon coupling: $g_\gamma = 0.0$ meV (blue rectangles) $g_\gamma = 0.1$ meV (red circles), $g_\gamma = 0.15$ meV (green diamonds). The temperature of the right lead is fixed at $T_R = 0.01$ K and tune the temperature. The Rashba coupling constant is $\alpha = 12.0$ meV nm (degeneracy energy point), the chemical potential of the leads are $\mu_L = \mu_R = 1.112$ meV, the magnetic field is $B = 10^{-5}$ T and $\hbar\Omega_0 = 1.0$ meV.

Rashba spin-orbit interaction can be used to fine tune the degeneracies and the thermal transport properties of the system. Note, that the thermal energy, the photon energy and the separation of the low lying states are all of a similar order of magnitude.

The heat and the thermoelectric currents are suppressed in the presence of a photon field due to an activation of photon replica states in the transport. The conceived Rashba spin-orbit influenced quantum ring system in a photon field could serve as a quantum device for optoelectronic applications with characteristics controlled by the Rashba constant, the electron-photon coupling strength, and the photon polarization.

Acknowledgments

This work was financially supported by the Research Fund of the University of Iceland, the Icelandic Research Fund, grant no. 163082-051. The calculations were carried out on the Nordic high Performance computer (Gardar). We acknowledge the University of Sulaimani, Iraq, and the Ministry of Science and Technology, Taiwan through Contract No. MOST 103-2112-M-239-001-MY3

References

- [1] S. Meir, C. Stephanos, T. H. Geballe, and J. Mannhart. Highly-efficient thermoelectronic conversion of solar energy and heat into electric power. *Journal of Renewable and Sustainable Energy*, 5(4):043127, 2013.
- [2] Joseph P. Heremans, Vladimir Jovovic, Eric S. Toberer, Ali Saramat, Ken Kurosaki, Anek Charoenphakdee, Shinsuke Yamanaka, and G. Jeffrey Snyder. Enhancement of Thermoelectric Efficiency in PbTe by Distortion of the Electronic Density of States. *Science*, 321(5888):554–557, 2008.

- [3] C. W. J. Beenakker and A. A. M. Staring. Theory of the thermopower of a quantum dot. *Phys. Rev. B*, 46:9667–9676, Oct 1992.
- [4] Feng Chi and Yonatan Dubi. Microwave-mediated heat transport in a quantum dot attached to leads. *Journal of Physics: Condensed Matter*, 24(14):145301, 2012.
- [5] R. Świrkowicz, M. Wierzbicki, and J. Barnaś. Thermoelectric effects in transport through quantum dots attached to ferromagnetic leads with noncollinear magnetic moments. *Phys. Rev. B*, 80:195409, Nov 2009.
- [6] S Fahlvik Svensson, A I Persson, E A Hoffmann, N Nakpathomkun, H A Nilsson, H Q Xu, L Samuelson, and H Linke. Lineshape of the thermopower of quantum dots. *New Journal of Physics*, 14(3):033041, 2012.
- [7] S Fahlvik Svensson, E A Hoffmann, N Nakpathomkun, P M Wu, H Q Xu, H A Nilsson, D Sánchez, V Kashcheyevs, and H Linke. Nonlinear thermovoltage and thermocurrent in quantum dots. *New Journal of Physics*, 15(10):105011, 2013.
- [8] Miguel A. Sierra, M. Saiz-Bretín, F. Domínguez-Adame, and David Sánchez. Interactions and thermoelectric effects in a parallel-coupled double quantum dot. *Phys. Rev. B*, 93:235452, Jun 2016.
- [9] L. W. Molenkamp, Th. Gravier, H. van Houten, O. J. A. Buijk, M. A. A. Mabesoone, and C. T. Foxon. Peltier coefficient and thermal conductance of a quantum point contact. *Phys. Rev. Lett.*, 68:3765–3768, Jun 1992.
- [10] Arafa H. Aly and C. K. Hwangbo. Electro-Thermal Transport in Quantum Point Contact Nanodevice. *International Journal of Thermophysics*, 30(2):661–668, 2009.
- [11] Allon I. Hochbaum, Renkun Chen, Raul Diaz Delgado, Wenjie Liang, Erik C. Garnett, Mark Najarian, Arun Majumdar, and Peidong Yang. Enhanced thermoelectric performance of rough silicon nanowires. *Nature*, 455:778–781, 2008.
- [12] M. Saiz-Bretín, A. V. Malyshev, P. A. Orellana, and F. Domínguez-Adame. Enhancing thermoelectric properties of graphene quantum rings. *Phys. Rev. B*, 91:085431, Feb 2015.
- [13] Zheng Jun, Chi Feng, Lu Xiao-Dong, and Zhang Kai-Cheng. Thermoelectric effect in an Aharonov-Bohm ring with an embedded quantum dot. *Nanoscale Research Letters*, 7(1):157–157, February 2012.
- [14] K Torfason, A Manolescu, S I Erlingsson, and V Gudmundsson. Thermoelectric current and Coulomb-blockade plateaus in a quantum dot. *Physica E*, 53:178–185, 2013.
- [15] Luca Vannucci, Flavio Ronetti, Giacomo Dolcetto, Matteo Carrega, and Maura Sassetti. Interference-induced thermoelectric switching and heat rectification in quantum Hall junctions. *Phys. Rev. B*, 92:075446, Aug 2015.
- [16] A. Dyrdał, M. Inglot, V. K. Dugaev, and J. Barnaś. Thermally induced spin polarization of a two-dimensional electron gas. *Phys. Rev. B*, 87:245309, Jun 2013.
- [17] C. M. Wang, H. T. Cui, and Q. Lin. Current-induced spin polarization for a general two-dimensional electron system. *physica status solidi (b)*, 246(10):2301–2306, 2009.
- [18] Li Xu, Zhi-Jian Li, Pengbin Niu, and Yi-Hang Nie. Nonequilibrium spin-polarized thermal transport in ferromagnetic-quantum dot-metal system.
- [19] Nzar Rauf Abdullah, Chi-Shung Tang, Andrei Manolescu, and Vidar Gudmundsson. *ACS Photonics*, 3(2):249–254, 2016.
- [20] Nzar Rauf Abdullah, Chi-Shung Tang, Andrei Manolescu, and Vidar Gudmundsson. Optical switching of electron transport in a waveguide-QED system. *Physica E: Low-dimensional Systems and Nanostructures*, 84:280–284, 2016.
- [21] Nzar Rauf Abdullah, Chi-Shung Tang, and Vidar Gudmundsson. Time-dependent magnetotransport in an interacting double quantum wire with window coupling. *Phys. Rev. B*, 82:195325, Nov 2010.
- [22] N. R. Abdullah. Magnetically and Photonically Tunable Double Waveguide Inverter. *IEEE Journal of Quantum Electronics*, 52(12):1–6, Dec 2016.
- [23] N R Abdullah, C S Tang, A Manolescu, and V Gudmundsson. Electron transport through a

- quantum dot assisted by cavity photons. *Journal of Physics:Condensed Matter*, 25:465302, 2013.
- [24] Thorsten Arnold, Chi-Shung Tang, Andrei Manolescu, and Vidar Gudmundsson. Magnetic-field-influenced nonequilibrium transport through a quantum ring with correlated electrons in a photon cavity. *Phys. Rev. B*, 87:035314, 2013.
- [25] Thorsten Arnold, Chi-Shung Tang, Andrei Manolescu, and Vidar Gudmundsson. Effects of geometry and linearly polarized cavity photons on charge and spin currents in a quantum ring with spin-orbit interactions. *The European Physical Journal B*, 87(5):113, 2014.
- [26] L. A. Thorsten. *The influences of cavity photons on the transient transport of correlated electrons through a quantum ring with magnetic field and spin-orbit interaction*. PhD thesis, School of Engineering and Natural Science, University of Iceland, Reykjavik, 2014.
- [27] V Gudmundsson, O Jonasson, Th Arnold, C.-S. Tang, H.-S. Goan, and A Manolescu. Stepwise introduction of model complexity in a general master equation approach to time-dependent transport. *Fortschr. Phys.*, 61:305, 2013.
- [28] Valeriu Moldoveanu, Andrei Manolescu, Chi-Shung Tang, and Vidar Gudmundsson. Coulomb interaction and transient charging of excited states in open nanosystems. *Phys. Rev. B*, 81:155442, Apr 2010.
- [29] M. Bagheri Tagani and H. Rahimpour Soleimani. . *Physica E*, 48:36–41, 2013.
- [30] Miguel A. Sierra and David Sánchez. Strongly nonlinear thermovoltage and heat dissipation in interacting quantum dots. *Phys. Rev. B*, 90:115313, Sep 2014.